

Dynamics of resonant phonons in ruby and alexandrite: A pair-state model

S. Majetich,* R. S. Meltzer, and J. E. Rives

Department of Physics and Astronomy, University of Georgia, Athens, Georgia 30602

(Received 27 June 1988)

Measurements of the escape time (lifetime), τ , of 29 and 37 cm^{-1} phonons from an optically excited volume in ruby ($\text{Al}_2\text{O}_3:\text{Cr}^{3+}$) and alexandrite ($\text{BeAl}_2\text{O}_4:\text{Cr}^{3+}$), respectively, are presented and compared with a model which takes into account Raman scattering of the phonons by the exchange-coupled Cr^{3+} pair states. The model differs from previous attempts to describe the dynamics of 29- cm^{-1} phonons in ruby in that the Raman scattering is calculated from specific pair-state wave functions and energy levels. The resulting single-parameter model produces excellent fits to the experimental data for both ruby and alexandrite, despite the fact that the dynamical processes which lead to the phonon escape are quite different in the two systems. The pair-state model presented here also predicts that the Raman scattering is dominated by pairs which have one ion in the ${}^4A_2(\pm\frac{1}{2})$ states. Measurements of τ as a function of temperature in a magnetic field confirm this prediction.

I. INTRODUCTION

Many attempts have been made to understand the dynamics of 29 cm^{-1} phonons resonantly trapped in the $\bar{E}({}^2E) \rightarrow 2\bar{A}({}^2E)$ excited-state resonance of Cr^{3+} in weakly doped ruby.¹⁻¹¹ At low excited ion concentrations, $N^* \leq 10^{16} \text{ cm}^{-3}$, the phonons diffuse spatially from the excited volume. At high N^* , the resonant phonon lifetime τ becomes independent of N^* and R , the radius of the excited volume, due to the presence of spectral shifting which can shift the phonon outside the Cr^{3+} ion resonance. Several models have been proposed to explain the spectral shifting. Meltzer, Rives, and Egbert¹ ascribed the loss to resonant-phonon-assisted energy transfer (RPAET) due to exchange-coupled Cr^{3+} pairs (Meltzer-Rives model). Although it explained the saturation of τ at large N^* and its independence of spot diameter R , the model required that the exchange parameter J be an order of magnitude less than previous estimates.^{12,13} Goossens, Dijkhuis, and de Wijn⁶ assumed the spectral shifting was due to Raman scattering by exchange-coupled Cr^{3+} pairs (de Wijn-Dijkhuis model). The de Wijn-Dijkhuis model properly described the dependence of τ on N^* for low and intermediate values of N^* , but failed to predict the total saturation of τ at large N^* . Happek, Holstein, and Renk^{10,11} attributed the spectral shifting to Raman shifting of the phonon frequencies by components of the ground manifold of Cr^{+2} ions.

Experiments by Basun, Kaplyanskii, and Feofilov¹⁴ studying time resolved fluorescence from the wings of the R_1 and R_2 lines under the influence of heat pulses, have shown that it is the resonant 29 cm^{-1} phonons coupling the \bar{E} and $2\bar{A}$ levels which are responsible for the population redistribution which follows the heat pulses. These experiments probe the exchange-coupled pairs whose energy splittings are in the 1–10 cm^{-1} range. Unfortunately, since the Cr^{3+} ions were excited in the broadband absorption, which excites both the single ions and the exchange-coupled pairs, it was not possible to distinguish RPAET from resonant Raman scattering of the 29 cm^{-1}

phonons. In a related, higher resolution, experiment which probed the more weakly exchange-coupled pairs using time-resolved fluorescence line-narrowing (FLN) techniques van Dort, Dijkhuis, and deWijn¹⁵ observed the spectral shifting of $\approx 29 \text{ cm}^{-1}$ phonons, injected with heat pulses, in the vicinity ($\pm 0.05 \text{ cm}^{-1}$) of the $\bar{E} \rightarrow 2\bar{A}$ resonance. Rapid spectral redistribution of the resonant and near-resonant phonons was evident in these measurements, but as in the previously mentioned results of Basun *et al.*¹⁴ it was not possible to determine whether the frequency shifting mechanism was dominated by RPAET or one-site resonant Raman processes.

However, Wietfeldt *et al.*¹⁶ have unambiguously shown in $\text{SrF}_2:\text{Er}^{3+}$ that RPAET is the dominant energy-transfer mechanism above 10 K. They were able to show, from the temperature dependence of the energy-transfer rate between energetically inequivalent Er^{3+} ions in a specific dimer pair, that the transfer must be assisted by resonant phonons which couple the two lowest-lying crystal-field levels of the initially excited ions.

Here the problem is reexamined experimentally and theoretically. The resonant phonon lifetime τ is measured over a wide range of N^* and R for both ruby ($\text{Al}_2\text{O}_3:\text{Cr}^{3+}$) and alexandrite ($\text{BeAl}_2\text{O}_4:\text{Cr}^{3+}$). Because of large differences in the parameters describing the excited-state resonance in these two systems, a comparison between them constitutes a good test of any model for phonon dynamics. The experimental results are analyzed in both systems and compared with computer simulations based on a new and more general description of the Cr^{3+} exchange-coupled pairs. The Meltzer-Rives and the de Wijn-Dijkhuis models are special cases of this new pair-state model. This new model successfully describes the lifetime τ as a function of N^* and R in both systems over the full range of N^* . In addition, the new model predicts, and new experiments corroborate, the temperature dependence of the phonon lifetime in ruby in a magnetic field. The model predicts that the rate of inelastic scattering by a Cr^{3+} pair depends on the spin

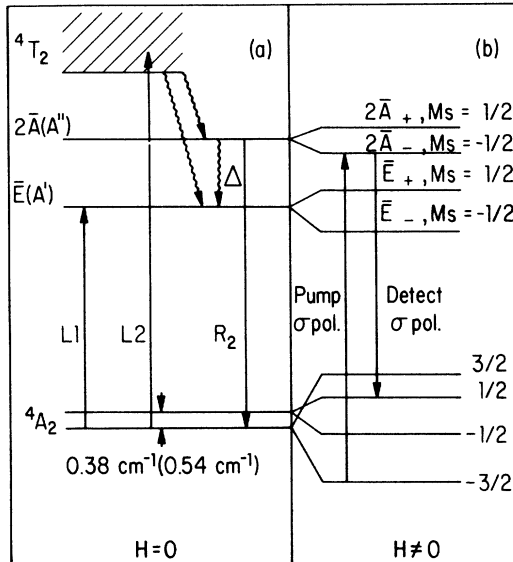


FIG. 1. Energy level diagram for ruby and alexandrite. At $H=0$ (a) the pumping scheme for laser 1 (L1) and laser 2 (L2) and the detection (R_2) is indicated. For ruby (b) in a magnetic field the pumping and detection schemes are indicated by the vertical arrows.

components M_S of the ion in the ground state and the specific predictions are consistent with experiment.

II. EXPERIMENT

In this work, resonant phonons are created and detected optically as illustrated in Fig. 1(a). To measure τ as a function of N^* and R , the R_1 transition of ruby (alexandrite) is first pumped creating a large population of Cr^{3+} ions in the metastable $\bar{E}(A')$ level which can absorb resonant phonons. One microsecond later a second laser pumps the broadbands (4T_2). The time delay is necessary to avoid heating effects from the intense first laser. Cr^{3+} ions excited into the broadbands undergo subnanosecond relaxation to either the $2\bar{A}(A'')$ or the $\bar{E}(A')$ level. The resulting excitations in the $2\bar{A}(A'')$ level relax rapidly to $\bar{E}(A')$, creating phonons of energy $\Delta=29$ (37) cm^{-1} . The intrinsic $2\bar{A} \rightarrow \bar{E}(A'' \rightarrow A')$ nonradiative decay time is $T_1=1.0$ ns in ruby¹⁷ (0.4 ns in alexandrite).¹⁵⁻¹⁸ The resonant phonons created by this decay are strongly scattered by multiple absorptions and reemissions by other Cr^{3+} ions in the metastable $\bar{E}(A')$ level which results in resonant trapping and prolonged containment in the excited region of the crystal.

The phonon population is monitored indirectly (see Fig. 1) by measuring the time dependence of the R_2 fluorescence signal which is proportional to the resonant phonon occupation number $\bar{p}(\Delta)$. The R_2 fluorescence is isolated with a Spex 0.75 m monochromator and detected by an Amperex 56 TVP photomultiplier tube. Signal averaging is accomplished with a Bionation 6500 transient digitizer interfaced to an LSI 11/23 computer.

In alexandrite the absorption and fluorescence was maximized¹⁹ by pumping with both lasers polarized parallel to the b axis, and viewing with c axis polarization. In ruby the pump laser and the fluorescence were

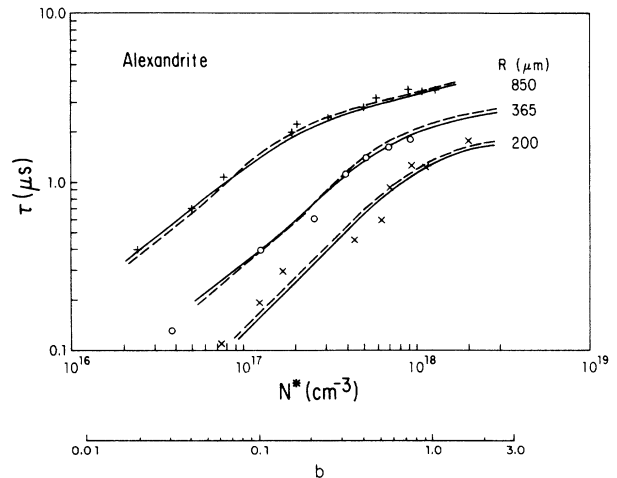


FIG. 2. Resonant (37 cm^{-1}) phonon lifetime in alexandrite as a function of N^* and bottleneck factor b at three values of the excited volume radius. Experimental data (+, O, X), wipeout model (---), pair-state model (—).

both polarized perpendicular to the c axis.

The excited-ion concentration N^* is obtained from the laser power R and absorption coefficient. The radius of the excited region is accurately controlled (± 0.002 mm) by placing a movable pinhole slide immediately before the crystal inside the cryostat.

III. RESULTS

At very short times (0–100 ns) after broadband pumping, the R_2 decay is nonexponential due to ballistic loss (escape without scattering) of phonons created near the boundaries of the excited region. This is followed by several decades of exponential decay, which we fit to determine τ . At still longer times slowly decaying tails result from heating of the excited volume by the absorbed laser pulse and thus the excited volume cools slowly. Figures 2 and 3 illustrate our results for the resonant phonon

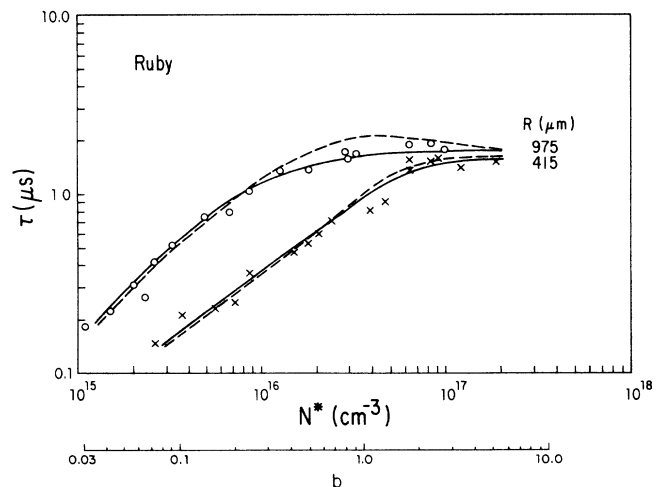


FIG. 3. Resonant (29 cm^{-1}) phonon lifetime in ruby as a function of N^* and bottleneck factor b at two values of the excited volume radius. Experimental data (O, X), wipeout model (---), pair-state model (—).

relaxation time τ as a function of N^* and R for alexandrite (0.054 at. % Cr) and ruby (0.08 at. % Cr). In general τ increases with increasing N^* and R . In addition to the data shown in Figs. 2 and 3 the dependence of τ on R was determined for both samples at several values of N^* .

The data for both samples can be separated into two distinct regions. In alexandrite (Fig. 2) for $N^*R \leq 10^{13}$ cm^{-2} , $\tau \cong N^{*0.8} R^{1.7}$. For $N^*R > 10^{13}$ cm^{-2} both the N^* and R dependencies are reduced. In ruby (Fig. 3) for $N^*R \leq 4 \times 10^{13}$ cm^{-2} , $\tau \cong N^{*0.7}$ and the R dependence decreases from $R^{0.9}$ to $R^{0.3}$ as N^* increases. For $N^*R > 4 \times 10^{13}$ cm^{-2} τ becomes independent of N^* and R , in agreement with earlier measurements.¹

IV. PHONON LOSS MECHANISMS

The loss by spatial transport is governed by scattering of the resonant phonons by the $\text{Cr}^{3+} \bar{E} \leftrightarrow 2\bar{A} (A' \leftrightarrow A'')$ transition. The mean free path for the process, $\lambda = v\tau_{\text{res}}$, where v is the speed of sound and τ_{res} is the ballistic propagation time of the phonon between emission and resonant reabsorption, can be expressed as

$$\lambda = vT_1/b, \quad (1)$$

where the bottleneck factor, $b = N^*/\Sigma$, and $\Sigma = 4\pi\omega^2\Gamma_{\text{res}}/v^3$ is the number of phonon modes within the $\bar{E} \leftrightarrow 2\bar{A} (A' \leftrightarrow A'')$ resonance width Γ_{res} at frequency ω . From previous measurements²⁰ Γ_{res} (ruby) = 0.02 cm^{-1} and Γ_{res} (alexandrite) = 0.43 cm^{-1} ; hence $\Sigma_{\text{ruby}} = 3 \times 10^{16}$ cm^{-3} and $\Sigma_{\text{alex}} = 1 \times 10^{18}$ cm^{-3} , and therefore $\lambda < R$ for the entire range of N^* and R used in these measurements. Thus the spatial loss is limited by a "random-walk" process rather than pure ballistic propagation.

In the limit where $\lambda \ll R$ the escape time is equal to the product of the time per step, $T_1 + \tau_{\text{res}}$, and the number of steps $(R/\lambda)^2$ which can be expressed as

$$\tau_{\text{dif}} = (R/v)^2 b(b+1)/T_1. \quad (2)$$

The factor $(b+1)^{-1} = \tau_{\text{res}}/(T_1 + \tau_{\text{res}})$ can be described physically as the fraction of time the excitation energy exists as a phonon. Thus the measured lifetime is always a factor $b+1$ greater than the intrinsic lifetime.

In this diffusive limit it is predicted that $\tau_{\text{dif}} \approx N^*R^2$ which suggests that the alexandrite data for $N^*R \leq 10^{13}$ cm^{-2} is dominated by spatial diffusion due to resonant emission and reabsorption, accompanied perhaps by spectral shifting within the $A'' \rightarrow A'$ resonance width. In fact, Eq. (2) yields values of τ within about 10 percent of the experimental values for $b = 0.1$ in alexandrite.

However, in ruby the weak dependence of τ on R indicates that additional loss mechanisms are important over the entire range of N^* and R used in this experiment. Therefore the effect of spectral shifting must be considered over the full range of N^* in ruby and at large N^* in alexandrite.

The anharmonic decay time of 29 cm^{-1} phonons in ruby has been independently estimated^{3,4} to be greater than 4 μs . The measured anharmonic lifetimes, $\tau_{\text{expt}} = \tau_{\text{anh}}(b+1)$, would be linear in N^* and independent

of R and would yield lifetimes an order of magnitude greater than observed. It is also anticipated that anharmonic processes of 37 cm^{-1} phonons in alexandrite will not be the dominant spectral shifting process based on the strong R dependence of τ_{expt} shown in Fig. 2.

From the above arguments it is clear that there are other spectral shifting mechanisms which are important in both ruby and alexandrite. A simple model is first considered where a single inelastic scattering process shifts the phonon frequency completely out of resonance with the $\bar{E} \leftrightarrow 2\bar{A} (A' \leftrightarrow A'')$ transition frequency. This is referred to as wipeout, following the notation first introduced by Goossens *et al.*,⁶ since the phonon can thereafter escape from the excited volume in a single ballistic step.

Given a probability of wipeout per random walk step P_{wo} then the wipeout rate is given by

$$\tau_{\text{wo}}^{-1} = (P_{\text{wo}}/T_1)b(b+1)^{-1}, \quad (3)$$

where the time per step, $T_1 + \tau_{\text{res}} = T_1(b+1)/b$. In this simple model the total phonon loss rate is the sum of the diffusive and wipeout rates.

$$\tau^{-1} = \tau_{\text{dif}}^{-1} + \tau_{\text{wo}}^{-1}. \quad (4)$$

Rough fits to the data for ruby and alexandrite are obtained for $R_{\text{eff}} \cong 1.5R$ and $\tau_{\text{wo}}^{-1} \cong 10^{-4}$ per step. The main feature of this simple model is that the spectral shifting due to wipeout does successfully predict a saturation of τ in ruby and a decrease in the N^* dependence of τ in alexandrite at large N^* . This simple model points to the importance of spectral shifting in the phonon loss.

In order to achieve a better understanding of the phonon dynamics it is desirable to produce a model which treats the resonant scattering process and the spectral shifting more exactly in view of the facts that the calculated mean free path for resonant scattering at the smallest N^* is of the order of R in alexandrite, and that small spectral shifts within the resonance should be important.

In Sec. V two computer simulation models are presented for the spatial random walk in the presence of inelastic scattering. In the first, an ad hoc introduction of inelastic scattering produces spectral wipeout with a fixed probability. In the second, the spectral wipeout is calculated from a model for Raman scattering of the phonons by the Cr^{3+} pairs, where the distribution of spectral shifts and resulting phonon mean free paths are explicitly computed.

V. COMPUTER SIMULATIONS

Lax *et al.*²¹ successfully demonstrated the use of computer simulations to study phonon dynamics in GaAs in the presence of elastic (isotope) scattering and inelastic (anharmonic) processes. In the present case a phonon random walk due to resonant scattering with the possibility of spectral shifting at each scattering event is considered. Spectral shifting is accompanied by a change in the probability of resonant scattering, and thus a change in the random-walk mean free path.

A phonon is created at a random initial position within the cylindrical excited volume and given a random direc-

tion and a random step size, based on an exponential distribution²² whose average is λ , the mean free path. Initially all of the resonant phonons are assumed to have the same mean free path, $\lambda_0 = vT_1 \Sigma / N^*$.

After each step it is determined whether the phonon has escaped from the excited volume. If not, the model determines whether, or not, to shift the frequency, and if so by how much, based on the probabilities determined from the model. If the frequency is shifted by $\delta\omega$, the new mean free path is

$$\lambda(\omega) = \lambda_0 / g(\omega), \quad (5)$$

where a Gaussian linewidth $g(\omega) = \exp(-4 \ln 2 \delta\omega^2 / \Gamma^2)$ is assumed where Γ is the excited state resonance full width at half maximum (FWHM). The number of phonons remaining in the excited volume is monitored as a function of time in order to determine the lifetime.

When the simulations are carried out with zero spectral shifting a good fit is obtained for alexandrite for values of N^* throughout the linear range of the data in Fig. 2, confirming the dominance of pure spatial diffusion in this range of N^* . However, it was not possible to fit the ruby data over any range of N^* , which supports our earlier suggestion that spectral shifting must be important over the entire range of N^* covered in this experiment.

A. Wipeout model

When spectral shifting is introduced via wipeout, the fits to the data shown by the dashed curves in Figs. 2 and 3 are obtained by choosing an intrinsic wipeout probability of 7.0×10^{-5} per step in alexandrite and 8.3×10^{-4} per step in ruby. Although this empirical model produces a very good fit to the alexandrite data over the entire range of N^* and R , it is only moderately successful in ruby in that it predicts too large a value for τ as saturation is approached, as seen in Fig. 3.

One reason for this behavior is the fact that this empirical wipeout model ignores any effect of small spectral shifts which leave the shifted phonon frequency in the wings of the $\bar{E} \leftrightarrow 2\bar{A}$ ($A' \leftrightarrow A''$) resonance. In ruby, with a resonance width of only 0.02 cm^{-1} , small spectral shifts will lead to a large increase in the resonant mean free path, and thus to an increased loss rate in comparison to that predicted by the wipeout model. Since the resonance width is 0.43 cm^{-1} in alexandrite,²⁰ small spectral shifts

will have a much smaller effect on the resonant mean free path and the phonon loss rate.

The wipeout model, though empirical by nature, does point to the importance of spectral shifting on the phonon dynamics in both ruby and alexandrite. Indeed the reasonable success of the wipeout model provided the necessary interest in seeking a more fundamental model of spectral shifting which involves a quantitative study of the effect of the exchange coupled Cr^{3+} pair states on the dynamics of the resonant phonons.

B. Pair-state model

In the pair-state model phonons may be inelastically scattered by exchange-coupled Cr^{3+} pairs, as with previous models, but here the pair-state wave functions and energy levels are treated explicitly. The pairs of interest have one ion in the ground state (4A_2) and the other in the first excited state (2E). Unlike earlier models the contributions to spectral diffusion of pairs with one ion in one of the ${}^4A_2(\pm\frac{1}{2})$ or ${}^4A_2(\pm\frac{3}{2})$ ground-state spin levels are differentiated. The interest here is in weakly coupled pairs where the exchange interaction may be treated as a perturbation. If the pairs are strongly coupled, the energy level splittings are no longer nearly resonant with the phonons created by the single ions, so these pairs will play no role in the resonant phonon dynamics.²³ Ruby which has a higher site symmetry is first tested and then the model is extended to alexandrite.

Pair states are first generated with single ion wave functions for a Cr^{3+} ion with cubic (O) site symmetry. This approach is chosen to take advantage of earlier results for the electronically equivalent V^{2+} ion.²⁴ The Hamiltonian for the exchange interaction is

$$H = -2 \sum_{i=1}^3 \sum_{j=1}^3 J_{ij} s_i^a \cdot s_j^b, \quad (6)$$

where s_i^a is the spin of electron i at site a , etc., and $i=1$ corresponds to $\xi(d_{yz})$, $i=2$ to $\eta(d_{xz})$, and $i=3$ to $\zeta(d_{xy})$ in the Tanabe and Sugano notation.²⁵ J_{ij} is one of the nine two-electron exchange parameters. The diagonal (ground-state) exchange parameter J is given by

$$J = \frac{1}{9} \sum_{i=1}^3 \sum_{j=1}^3 J_{ij}. \quad (7)$$

Strictly speaking, this interaction involves superexchange

TABLE I. Pair-state basis functions for ${}^2E(\bar{E})$ and ${}^2E(2\bar{A})$. The $u \pm$ wave functions are linear combinations of product wave functions $|\xi\eta\zeta\rangle$ which transform as irreducible representations of the double group \bar{C}_3 . (ξ , η , and ζ are related to the d orbitals d_{yz} , d_{xz} , and d_{xy} , respectively.) For further details, see Ref. 22.

For $n = 1, 3, 5, 7^a$

$$|\psi_n^{\bar{E}}\rangle = |{}^2E_{u-\frac{1}{2}} A_2 M_s\rangle, \text{ where } M_s = (4-n)/2, |\psi_n^{2\bar{A}}\rangle = |{}^2E_{u+\frac{1}{2}} A_2 M_s\rangle$$

For $n = 9, 11, 13, 15^a$

$$|\psi_n^{\bar{E}}\rangle = |{}^2E_{u+} - \frac{1}{2} A_2 M_s\rangle, \text{ where } M_s = (12-n)/2, |\psi_n^{2\bar{A}}\rangle = |{}^2E_{u-} - \frac{1}{2} A_2 M_s\rangle$$

^aEven-numbered basis states are obtained from their $n-1$ counterpart by interchanging the ions in the ground and excited states, e.g., $|\psi_2^{\bar{E}}\rangle = |{}^4A_2 \frac{3}{2} E_{u-\frac{1}{2}}\rangle$.

TABLE II. Pair-state energy matrices (each letter in a block represents a unique 2×2 matrix defined in Tables III and IV; see * symbols) in the pair-state representation for the \bar{E} and $2\bar{A}$ (the matrix for the $2\bar{A}$ pair states is obtained from that for the \bar{E} state by taking the complex conjugate of all 2×2 blocks except for the f block which is the same) states.

m	1,2	3,4	5,6	7,8	9,10	11,12	13,14	15,16
n								
1,2	a^*							
3,4		b^*			e^*			
5,6			c^*			f		
7,8			d^*				g^*	
9,10		e			d			
11,12			f^*			c		
13,14			g			b		
15,16								a

TABLE III. Coefficients in the expressions for the matrix elements appearing in the a , b , c , and d 2×2 blocks of the energy matrix. (The quantities R_1 and I_1 are defined in Table V.) $q_{ij} = \Delta/2q_{ij}^{\Delta} + \epsilon/2q_{ij}^{\epsilon} + \delta/2q_{ij}^{\delta} + Jq_{ij}^J + R_1q_{ij}^{R_1} + iI_1q_{ij}^{I_1}$, where $q_{22} = q_{11} - \delta$; $q_{21} = q_{12}^*$.

q_{ij}	q_{ij}^{Δ}	q_{ij}^{ϵ}	q_{ij}^{δ}	q_{ij}^J	$q_{ij}^{R_1}$	$q_{ij}^{I_1}$
a_{11}	1	-1	1	$-\frac{1}{6}$	0	0
a_{12}	0	0	0	0	$-\frac{1}{3}$	$\sqrt{3}/6$
b_{11}	1	1	1	$-\frac{1}{9}$	0	0
b_{12}	0	0	0	0	$-\frac{4}{9}$	$2\sqrt{3}/9$
c_{11}	1	1	1	$\frac{1}{9}$	0	0
c_{12}	0	0	0	0	$-\frac{2}{9}$	$\sqrt{3}/9$
d_{11}	1	-1	1	$\frac{2}{3}$	0	0
d_{12}	0	0	0	0	0	0

TABLE IV. Coefficients in the expressions for the matrix elements appearing in the e , f , and g 2×2 blocks of the energy matrix. (The quantities R_2 , I_2 , R_3 , and I_3 , are defined in Table V.) $q_{ij} = R_2q_{ij}^{R_2} + iI_2q_{ij}^{I_2} + R_3q_{ij}^{R_3} + iI_3q_{ij}^{I_3}$, where $q_{22} = q_{11}$ by replacing R_2 with R_2' and I_2 with I_2' and $q_{21} = q_{12}$.

q_{ij}	$q_{ij}^{R_2}$	$q_{ij}^{I_2}$	$q_{ij}^{R_3}$	$q_{ij}^{I_3}$
e_{11}	$2\sqrt{3}/9$	$7\sqrt{3}/18$	0	0
e_{12}	0	0	$\sqrt{3}/9$	$1/3$
f_{11}	$4/9$	3	0	0
f_{12}	0	0	$-4/9$	$2/9$
g_{11}	$4\sqrt{3}/9$	$2/3$	0	0
g_{12}	0	0	$-2\sqrt{3}/9$	$\sqrt{3}/9$

TABLE V. Coefficients α_{ij}^Q defining the specific linear combinations of two-electron exchange parameters which appear in the 2×2 blocks of the energy matrices. $Q = \sum_{i,j=1}^3 \alpha_{ij}^Q J_{ij}$.

$Q \setminus ij$	11	22	33	12	21	13	31	23	32
R_1	1	1	1	$-\frac{1}{2}$	$-\frac{1}{2}$	$-\frac{1}{2}$	$-\frac{1}{2}$	$-\frac{1}{2}$	$-\frac{1}{2}$
R_2	1	1	-2	1	1	1	-2	1	-2
R_2'	1	1	-2	1	1	-2	1	-2	1
R_3	$-\frac{1}{2}$	$-\frac{1}{2}$	1	1	1	$-\frac{1}{2}$	$-\frac{1}{2}$	$\frac{1}{2}$	$\frac{1}{2}$
I_1	0	0	0	-1	1	1	-1	-1	1
I_2	-1	1	0	-1	1	-1	0	1	0
I_2'	-1	1	0	1	-1	0	-1	0	1
I_3	1	-1	0	0	0	-1	-1	1	1

because the Cr^{3+} ions are coupled through intervening O^{2-} ions. Exchange matrix elements in the cubic basis are calculated for pair states with one ion in the ground state and the second in the first excited state (2E). The sixteen pair state basis functions for ruby and their exchange matrix elements in the C_3 double group basis are determined with the appropriate symmetry transformation operations and the use of raising and lowering operators as shown in Tables I–V.

Considering the site-site energy difference δ between the two sites due to inhomogeneous broadening, the states $|E^a A^b\rangle \equiv |{}^2E^4 A_2\rangle$ and $|A^a E^b\rangle \equiv |{}^4A_2^2 E\rangle$ have different energies, so there are 32, not 16, different pair states. The distribution of δ is related to the (optical) width of the R_1 line since it describes the energy difference between the 2E and 4A_2 states. The site-site energy difference δ is included in the energy matrix by the addition of diagonal matrix elements, $+\delta/2$ for $|E^a A^b\rangle$ and $-\delta/2$ for $|A^a E^b\rangle$. The 2E crystal-field splitting Δ and the ground-state splitting ϵ between the $M_S = \pm\frac{1}{2}$ and $M_S = \pm\frac{3}{2}$ levels in the 32×32 energy matrix are specifically included. Mixing between the $(\bar{E}, {}^4A_2)$ and $(2\bar{A}, {}^4A_2)$ manifolds is ignored, so that the matrix can be reduced to two 16×16 blocks. They differ in only two off-diagonal elements (see caption of Table II). By diagonalizing these matrices the energy eigenvalues and the eigenfunctions for a pair with a particular exchange interaction and site-site energy mismatch, δ are determined.

The off-diagonal exchange parameters J_{ij} are very difficult to calculate for even a single type of pair, yet the contributions from a full range of pairs is required. Their values are approximated by randomly generating J_{ij} 's such that their sum equals the diagonal exchange parameter J . In this way a distribution function for each of the eight sums which appear repetitively in the off-diagonal elements is obtained. Because the J_{ij} 's can be either positive or negative, the absolute value is averaged when determining the relative size of the off-diagonal sums to J . Using this method, the most probable absolute value of most of the sums is found to be about 0.6 J. With this as a starting point, the two 16×16 matrices were used to determine the energy eigenvalues and eigenfunctions for a pair with given values of J and δ .

In the computer simulation, for each scattering event the probability $P(\Delta\omega)$ of spectral shifting by a frequency $\Delta\omega$ is required. These quantities for individual pairs are calculated, and the results are weighted according to the distribution of pairs with given values of J and δ .

To obtain the contribution to spectral from a particular pair, the overlap S for all 256 pair transitions, where S is the overlap of the pair transitions in the single-ion basis, are first calculated. Each pair-state eigenfunction, $|\phi_i^{\bar{E}}\rangle$ consists of a linear combination of the 16 orthonormal pair-state basis function, $|\psi_m^{\bar{E}}\rangle$ listed in Table I and is of the form

$$|\phi_i^{\bar{E}}\rangle = \sum_{m=1}^{16} a_{im}^{\bar{E}} |\psi_m^{\bar{E}}\rangle. \quad (8)$$

A similar result exists for the 16 pair states $|\phi_j^{2\bar{A}}\rangle$ in

terms of the basis functions $|\psi_m^{2\bar{A}}\rangle$. The pair state basis functions are numbered in such a way that only the $m=n$ transitions between the $|\psi_m^{2\bar{A}}\rangle$ and $|\psi_n^{\bar{E}}\rangle$ pair-state basis functions have nonzero overlap. These correspond to the spin-nonflip transitions of the single ion. Therefore

$$S_{ij} = \sum_{m=1}^{16} a_{im}^{\bar{E}} a_{jm}^{2\bar{A}}. \quad (9)$$

The probability that the pair will inelastically scatter a resonant phonon by an amount $\Delta\omega = \omega_{ij} - \omega_{jk}$, where ω_{ij} is the transition frequency between pair state $|\phi_i^{\bar{E}}\rangle$ and $|\phi_j^{2\bar{A}}\rangle$ (phonon absorption) and ω_{jk} is the transition frequency between $|\phi_j^{2\bar{A}}\rangle$ and $|\phi_k^{\bar{E}}\rangle$ (emission) is then calculated. The probability of inelastic scattering relative to that of elastic scattering by a single ion is

$$P(\Delta\omega, J, \delta) = \begin{cases} \frac{1}{16} |S_{ij}|^2 |S_{jk}|^2 & \text{if } |\omega - \omega_{ij}| < \Gamma/2 \\ 0 & \text{if } |\omega - \omega_{ij}| > \Gamma/2 \end{cases}. \quad (10)$$

The factor of $\frac{1}{16}$ accounts for the probability that the pair state $|\phi_i^{\bar{E}}\rangle$ will be occupied and the requirement on $\omega - \omega_{ij}$ allows scattering only when the incoming phonon is resonant with the pair transition $i \rightarrow j$, where Γ is the frequency width of the phonon distribution.

A pair with given values of J and δ will have a multiplicity of possible shifts $\Delta\omega$ each with a different probability. An average over all pairs is calculated. This is equivalent to averaging over the distribution of J and δ for the pairs. J and δ are treated independently and the average is first taken over the site-site energy difference δ yielding

$$P(\Delta\omega, J) = \int_0^\infty P(\Delta\omega, J, \delta) W(\delta) d\delta, \quad (11)$$

where the weighting function $W(\delta)$ is given by¹

$$W(\delta) = \int_0^\infty g(E)[g(E+\delta) + g(E-\delta)] dE. \quad (12)$$

The function $g(E)$ is the probability that a single Cr^{3+} ion has energy E and is given by

$$g(E) = (2\pi\Delta E^2)^{-1/2} \exp[-(E - E_0)^2 / 2\Delta E^2], \quad (13)$$

where ΔE is the R_1 inhomogeneous linewidth, 0.18 cm^{-1} in ruby¹ (0.8 cm^{-1} in alexandrite²⁰) and E_0 is the peak absorption energy. An exponential dependence of the exchange parameter on the ion separation r ,¹

$$J = J_0 e^{-ar}, \quad (14)$$

is assumed. The probability distribution of finding a pair with separation r in a randomly doped sample is

$$W(r) = 4\pi n_0 r^2 \exp(-4\pi n_0 r^3 / 3), \quad (15)$$

as determined by Lyo.²⁶

The borderline between single ions and pairs is chosen to be $r_{\text{max}} = 14 \text{ \AA}$, which corresponds to an exchange interaction of about $J_{\text{min}} = 2.5 \times 10^{-3} \text{ cm}^{-1}$. A pair separated by this distance behaves like two single ions. A minimum value of r for active pairs is chosen, because if $r < r_{\text{min}}$, no pair states are resonant with the 29 cm^{-1} phonons. For example, this is definitely the case for the

fourth-nearest-neighbor pairs, separated by 3.5 \AA .⁸ A value of $r_{\min} = 5.8 \text{ \AA}$, which corresponds to $J_{\max} = 1.0 \text{ cm}^{-1}$, is chosen.

Then $W(J)$, the probability of finding a pair with exchange interaction J , is obtained by combining Eqs. (14) and (15). The overall shifting probability $P(\Delta\omega)$ is obtained by integrating $P(\Delta\omega, J)$ weighted by $W(J)$ from J_{\min} to J_{\max} yielding

$$P(\Delta\omega) = \int_{J_{\min}}^{J_{\max}} P(\Delta\omega, J) W(J) dJ. \quad (16)$$

With these choices of r_{\min} and r_{\max} , for 0.08 wt. % ruby, 0.9% of the Cr^{3+} behave as strongly interacting pairs which do not absorb phonons of energy Δ , 12.7% of the ions behave as weakly interacting pairs which are the source of the spectral diffusion, and 86.4% behave as single ions which absorb resonant phonons but do not shift their frequency.

The scattering behavior of a pair can be qualitatively characterized by the ratio of J to δ . Figure 4 illustrates the energy levels of some typical pairs with different values of J/δ . For pairs with $J/\delta < 1$, in both the $(\bar{E}, {}^4A_2)$ and $(2\bar{A}, {}^4A_2)$ groups of pair states there are two sets of doubly degenerate energy levels separated by the $\bar{E}(2\bar{A})$ energy mismatch δ . At an energy ϵ (the single-ion ground-state splitting) above them is a group of closely spaced levels. The pair-state eigenfunctions ϕ of the lower levels consist of single pair-state basis functions ψ which include either the ${}^4A_2(\frac{3}{2})$ or the ${}^4A_2(-\frac{3}{2})$ ground state. These states behave as single-ion states; a phonon absorbed by one of them will be elastically scattered. The remaining pair-state eigenfunctions are linear combinations of basis states which include either the ${}^4A_2(\frac{1}{2})$ or the ${}^4A_2(-\frac{1}{2})$ ground state. Because of the mixing, these states are less likely to absorb a phonon than a single ion, but unlike a single ion they can shift the

phonon frequency. The size of the shift for a typical pair with $J/\delta < 1$ will be less than the half-width of the resonance Γ so the mean free path of the phonon will not be significantly altered.

As the ratio J/δ is increased, the pair-state energy level splittings increase, so the shifts which are allowed are more effective in changing the phonon mean free path. Also basis states ψ are further mixed so the net shifting probability increases. In the case of $J/\delta \gg 1$, basis states related by energy transfer, such as $|{}^2E_u - M_s, {}^4A_2 M_s\rangle$ and $|{}^4A_2 M_s, {}^2E_u - M_s\rangle$, may be mixed together in the same eigenstate, unlike the case where $J/\delta \leq 1$. The Meltzer-Rives model¹ considered spectral shifting only from such states, while the de Wijn-Dijkhuis model⁶ ignored the contribution from these states entirely. In contrast to the case for pairs with $J/\delta < 1$, when $J/\delta \gg 1$ inelastic scattering from pair states containing the ${}^4A_2(\pm\frac{3}{2})$ states dominates over the contribution from those containing the ${}^4A_2(\pm\frac{1}{2})$ states. Wipeout, rather than small shifts within the resonance width, typifies the spectral shifting in this case.

The calculated overall shifting probability $P(\Delta\omega)$, for ruby is shown in Fig. 5. The bar graphs (solid lines) are the calculated values as a function of shifting frequency and the dashed curves represent analytic approximations to the calculations which are of the form of a Gaussian ($\Gamma = 0.24 \text{ cm}^{-1}$) for $\Delta\omega < 0.3 \text{ cm}^{-1}$ and a constant for $\Delta\omega > 0.3 \text{ cm}^{-1}$. The $2\bar{A} \rightarrow \bar{E}$ ($A'' \rightarrow A'$) resonance width Γ_{ruby} is indicated by the arrow in Fig. 5. It is clearly seen that most of the inelastic scattering events in ruby lead to wipeout.

In the version of the pair-state model which fits the experimental results, the pair states which include an ion in the ${}^4A_2(+\frac{1}{2})$ or ${}^4A_2(-\frac{1}{2})$ ground state are responsible for 95% of the frequency shifts. The contributions from ${}^4A_2(+\frac{1}{2})$ and ${}^4A_2(-\frac{1}{2})$ are identical, as are those from ${}^4A_2(+\frac{3}{2})$ and ${}^4A_2(-\frac{3}{2})$. A combination of spin selection

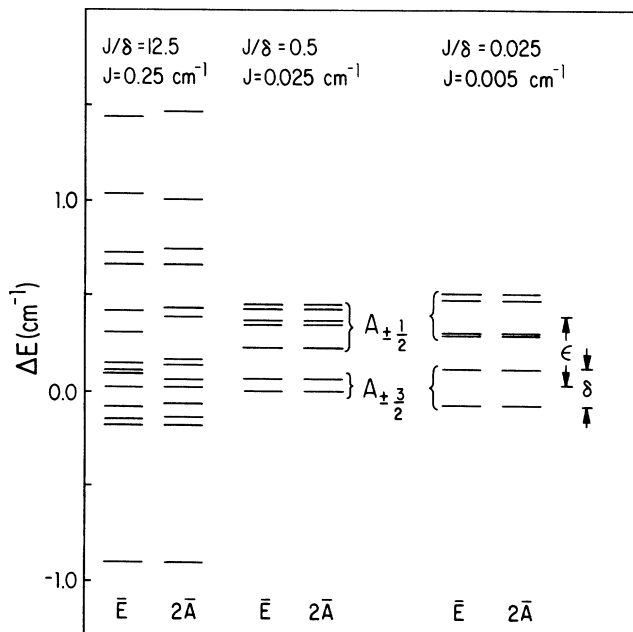


FIG. 4. Exchange-coupled pair-state energy levels in ruby relative to the single-ion energies for three values of J/δ .

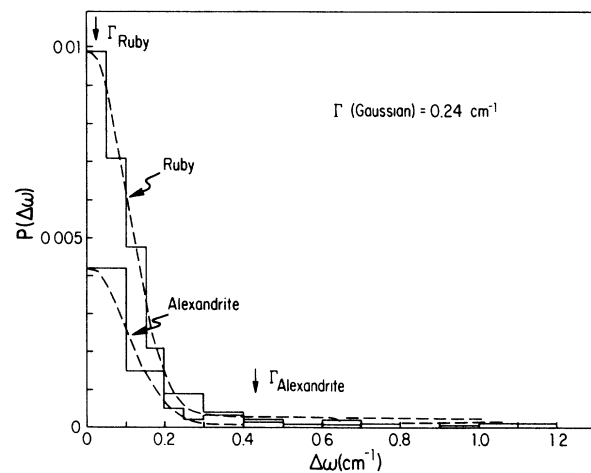


FIG. 5. Phonon frequency shifting probabilities for ruby and alexandrite from the pair-state model. The bar graphs are the calculated values as a function of frequency shift ($\Delta\omega$). The dashed curves are analytic approximations described in the text. The vertical arrows indicate the excited state resonance widths for ruby (Γ_{ruby}) and alexandrite ($\Gamma_{\text{alexandrite}}$).

rules and the relatively small size of the exchange matrix elements coupling ${}^4A_2(\pm\frac{3}{2})$ to other basis states leads to less mixing of the ${}^4A_2(\pm\frac{3}{2})$ basis states and therefore less spectral shifting from them except for pairs where $J/\delta \gg 1$.

The model is found to predict a bit too much spectral shifting to fit the experimental results. However, a slight reduction of the off-diagonal sums from the value 0.6 J, estimated above from the statistical average of many distribution of J_{ij} , to 0.5 J produces a good fit.

In the saturation region of the relaxation time in ruby (large N^*), spectral shifting is the only means of escape for phonons. Since all but the very smallest shifts lead to wipeout, as seen in Fig. 5, this is a highly probable process leading to a saturation in the phonon loss rate. If $P(\Delta\omega)$ for the very small shifts is altered the calculated phonon lifetime is effected very slightly, while small changes in $P(\Delta\omega)$ for the larger shifts (wipeout) change τ by orders of magnitude. The best results from the pair-state model for ruby are shown in Fig. 3 by the solid lines where they can be compared with the experimental data.

It is important to point out at this point that the pair-state model described above is essentially a *one*-parameter model. Once reasonable values of r_{\min} and r_{\max} are chosen, as discussed above, the only adjustable parameter is the most probable value of the sums of the off-diagonal exchange parameters J_{ij} which we chose to be 0.5 J to produce the best fit to the ruby data. It was however necessary to renormalize the values of N^* for the experimental data by about 50% in order to achieve the fit shown in Fig. 3. However this is the least reliable experimental parameter, and errors of 50% in its absolute value are to be expected. The relative values of N^* , however, are known to a much higher degree of accuracy.

In extending the pair-state model to alexandrite, several differences from ruby must be taken into account. In the first place, the exchange parameters are not necessarily the same in ruby and alexandrite. However, the exchange parameters for some strongly coupled pairs in alexandrite were found to lie between 4 and 7 cm^{-1} .²⁷ Although the pairs to which these values correspond are unknown, their values are similar in magnitude to that of the fourth nearest neighbors in ruby, $J=10 \text{ cm}^{-1}$.⁸ Therefore we take the same parameters for Eq. (14) as in ruby.

A second difference is the lower site symmetry C_5 of Cr^{3+} ions in alexandrite. In ruby single-ion basis states can be constructed for which M_S is a good quantum number and which transform as irreducible representations of the double group C_3 ; for alexandrite, basis functions which transform like irreducible representations of the C_5 double group no longer have M_S as a good quantum number. Calculation of the exchange matrix elements and the assignment of spin-nonflip (allowed) and spin flip (forbidden) absorptions are therefore impossible. The lowering of the Cr^{3+} site symmetry relaxes the spin selection rules for matrix elements in alexandrite, leading to more mixing of basis states in the eigenfunctions, and therefore more spectral diffusion. However, despite these facts the large differences in both the optical and excited state resonance linewidths are expected to dominate the

phonon dynamics. Therefore the phonon dynamics in alexandrite is modeled with the same basis functions and exchange parameters $J(\mathbf{r})$ as for ruby. While the inhomogeneous optical linewidth in alexandrite is four times great than in ruby, the excited-state resonance width is 20 times broader than in ruby.¹⁹ As a result, the typical value of δ increases by a factor of 4 but a phonon must be shifted in frequency by 20 times as far in order for wipeout to occur. The resulting shifting probability, $P(\Delta\omega)$, for alexandrite is shown in Fig. 5. It is clear that most inelastic scattering events in alexandrite leave the phonon within the $A'' \rightarrow A'$ resonance. In addition, since J/δ for alexandrite is typically one-fourth that in ruby, inelastic scattering will occur much less frequently in alexandrite as shown in Fig. 5.

Using the same pair-state model with the same values of the off-diagonal sums parameter, 0.5 J, as in ruby, the fit to the alexandrite data shown by the solid curves in Fig. 2 is obtained. As in the case of ruby, renormalization of the experimental values of N^* by about 50% was required. Thus, despite the lower symmetry and much broader optical and resonance linewidths in alexandrite, the resonant phonon dynamics in both systems can be understood using a single model of Raman shifting of the phonon frequencies within the Cr^{3+} pair states.

In the crude wipeout model, described above, it was necessary to introduce a wipeout probability in alexandrite which was an order of magnitude greater than in ruby in order to produce reasonable fits to the experimental data. The pair-state model requires a wipeout probability in ruby essentially the same as that used in the crude model, but in alexandrite the predicted probability is only three times that used in ruby because smaller frequency shifts relative to the resonance halfwidth Γ are more important in alexandrite. Whereas in ruby at high N^* , phonons escape predominantly by spectral shifting, in alexandrite phonons escape by a combination of spectral shifting and spatial diffusion.

VI. EXPERIMENTS IN A MAGNETIC FIELD

Although previous models have either ignored the ground-state splitting or have not determined the relative contributions from the different levels, the pair-state model differentiates the two ground-state spin levels and attributes the bulk of the spectral diffusion in ruby to Cr^{3+} ion pairs with one ion in the ${}^4A_2(\pm\frac{1}{2})$ states. This prediction is tested by applying a magnetic field to remove the degeneracy of the ground-state levels, as shown in Fig. 1(b). The field depletes the ${}^4A_2(\pm\frac{1}{2})$ population such that at 29 kG and 1.4 K the ${}^4A_2(-\frac{3}{2})$ level contains over 95% of the population. By varying the temperature between 1.4 and 2.2 K, the combined population of the ${}^4A_2(\pm\frac{1}{2})$ levels increases over three hundred percent. If the ${}^4A_2(\pm\frac{1}{2})$ states dominate the spectral shifting, as predicted by the pair-state model, the phonon loss rate should rise as the temperature is increased.

Placing the sample in a magnetic field complicates the phonon generation and dynamics. When pumping the $2\bar{A}$ level, phonons in two frequency groups are created,

one corresponding to a spin-flip and the other a spin-nonflip transition. Though the spin non-flip rate is fifteen times faster than the spin-flip rate,^{17,28} rate equation solutions of this system have indicated that the number of spin-flip and spin-nonflip phonons become about equal²⁹ because the spin-nonflip transition is much more bottlenecked than the spin flip transition. Effectively the two phonon packets equilibrate in "temperature."

To most clearly distinguish the contribution of the ground-state spin levels the magnetic-field experiments were performed in ruby under conditions of maximum spectral diffusion (high N^*). While the value of N^* could not be correlated exactly with values from earlier measurements, a lower limit of $2 \times 10^{17} \text{ cm}^{-3}$ is estimated, based on the dependence of the relaxation time on the laser power.

In a field it is possible to use a single laser to pump the $2\bar{A}$ level directly, as shown in Fig. 1(b), since the resonant phonon population can be monitored with the time dependence of the $2\bar{A}(-\frac{1}{2}) \rightarrow {}^4A_2(+\frac{1}{2})$ fluorescence which is not resonant with the exciting laser. Only for the temperature dependence at zero magnetic field is the original pumping scheme used to minimize scattered light.

The phonon loss rate τ^{-1} increases almost linearly with temperature, as shown in Fig. 6 for four magnetic fields. This is expected if the ${}^4A_2(\pm\frac{1}{2})$ pair states dominate the spectral diffusion because their populations increase almost linearly with temperature in this region. The slope

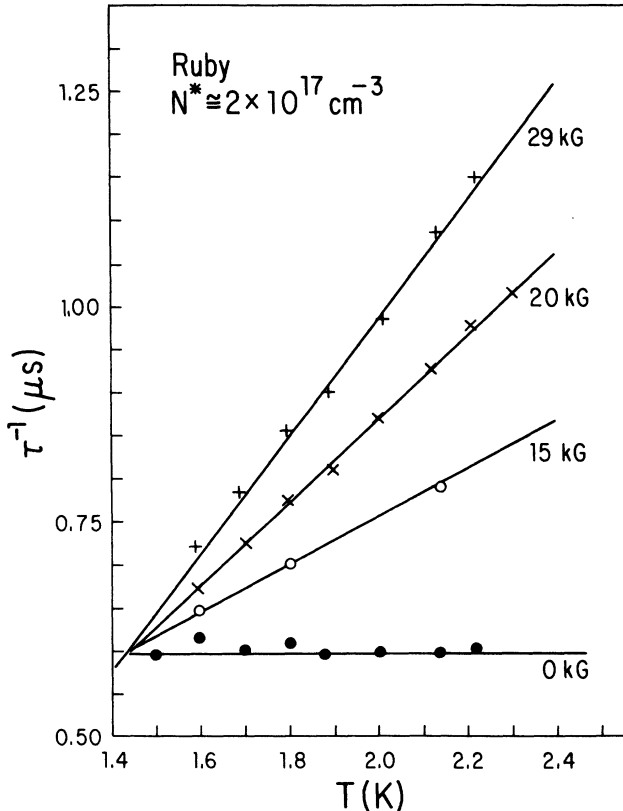


FIG. 6. Temperature dependence of the 29 cm^{-1} phonon lifetime in ruby at several values of the magnetic field using the pumping and detection scheme indicated in Fig. 1(b).

increases with increasing magnetic field because the rate of change of the ${}^4A_2(\pm\frac{1}{2})$ population with temperature is roughly proportional to the magnetic field.

In the pair-state model the spectral diffusion rates, $\tau_{\pm 3/2}^{-1}$ and $\tau_{\pm 1/2}^{-1}$, due to the ${}^4A_2(\pm\frac{1}{2})$ and ${}^4A_2(\pm\frac{3}{2})$ sets of pair states are independent of each other, are constant for a given magnetic field and satisfy the constraints $\tau_{3/2}^{-1} = \tau_{-3/2}^{-1}$, and $\tau_{1/2}^{-1} = \tau_{-1/2}^{-1}$. The experimental relaxation rate equals a weighted sum of the rates for the two types of pairs, where the weighting factors are the occupations of the ${}^4A_2(\pm\frac{1}{2})$ and ${}^4A_2(\pm\frac{3}{2})$ levels, $\bar{n}_{\pm 1/2}$ and $\bar{n}_{\pm 3/2}$, respectively. Therefore the total spectral diffusion rate is

$$\begin{aligned} \tau^{-1}(T, H) = & \tau_{\pm 3/2}^{-1}(H) [\bar{n}_{3/2}(T, H) + \bar{n}_{-3/2}(T, H)] \\ & + \tau_{\pm 1/2}^{-1}(H) [\bar{n}_{1/2}(T, H) + \bar{n}_{-1/2}(T, H)] . \end{aligned} \quad (17)$$

The data of Fig. 6 are fit with Eq. (17) to determine the two unknowns, $\tau_{\pm 1/2}^{-1}(H)$ and $\tau_{\pm 3/2}^{-1}(H)$. The results are shown by the closed circles in Fig. 7 where it is seen that the contribution from the ${}^4A_2(\pm\frac{1}{2})$ pair states dominate, and the relative importance of the ${}^4A_2(\pm\frac{1}{2})$ states rises with increasing magnetic field.

In order to gain a better theoretical understanding of this result the pair-state model is used to calculate shifting probabilities for some typical pairs as a function of the magnetic field. Since the shifting probability is directly proportional to the intrinsic spectral diffusion rate, the effect of a magnetic field can be determined

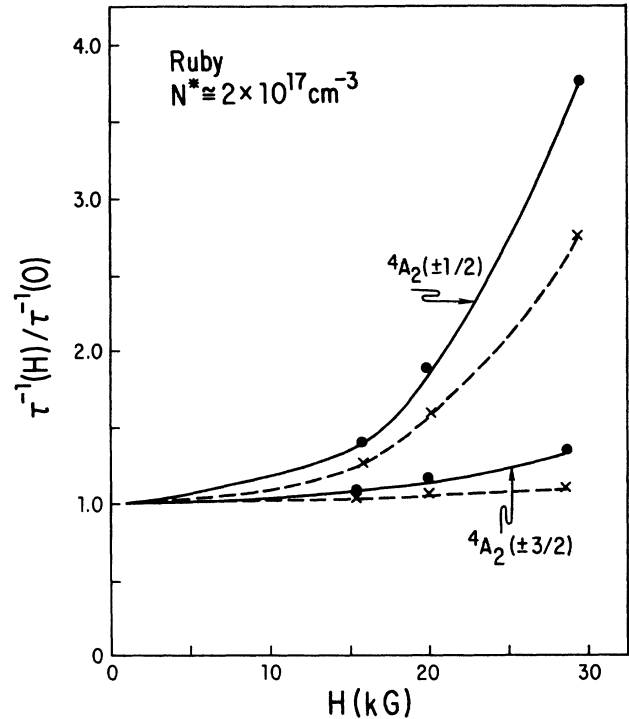


FIG. 7. Magnetic-field dependence of the 29 cm^{-1} phonon frequency shifting rates ($\tau_{\pm 1/2}^{-1}$ and $\tau_{\pm 3/2}^{-1}$) in ruby calculated from the experimental data and Eq. (17) (●) and calculated from the pair-state model (×).

without actual simulations of the phonon dynamics. The appropriate Zeeman terms are added along the diagonal of the two 16×16 energy matrices and new eigenvalues and eigenfunctions are determined in the magnetic field. The possible absorption and emission routes are determined using the concepts of resonance and overlap described earlier, except that in a magnetic field there are two types of resonant phonons. In accordance with the rate equations for large N^* ,²⁹ both are assumed to be equally populated. After summing the probabilities for the allowed absorption and emission pathways which shift the phonon frequency, the net shifting probability is calculated.

The calculations show that between 0 and 29 kG, the spectral diffusion rate from the pairs containing ${}^4A_2(\pm\frac{1}{2})$ nearly triples while that for pair states containing ${}^4A_2(\pm\frac{3}{2})$ remains constant. This result, shown by the crosses in Fig. 7, is in remarkable agreement with the analysis of the experimental observations.

The reason for the different magnetic-field dependence of the spectral diffusion rates for pair states containing ${}^4A_2(\pm\frac{3}{2})$ and those containing ${}^4A_2(\pm\frac{1}{2})$ is easy to understand. The basis functions containing ${}^4A_2(\pm\frac{3}{2})$ are only very weakly coupled to other basis states except for their energy-transfer related state. However, the energy-transfer states both have the same diagonal Zeeman terms, so the resulting eigenfunctions are unchanged in a magnetic field. They also have the same M_s value, so the size of the shifts does not vary with magnetic field. On the other hand, the ${}^4A_2(\pm\frac{1}{2})$ basis functions mix considerably with each other, including functions with different values of M_s . This increases the shift sizes as the magnetic field increases, making wipeout more probable. These experiments in a magnetic field support the pair-state model in that they verify the importance of the M_s value of the ground state in determining the spectral diffusion rate, as predicted by the model.

VII. CONCLUSIONS

The lifetimes of nonequilibrium distributions of 29 and 37 cm^{-1} phonons in ruby and alexandrite, respectively, have been measured as a function of Cr^{3+} excited-state concentration, N^* , and excited volume radius R . In addition, the temperature dependence of the lifetime in a magnetic field was measured for the first time. The phonon dynamics were found to be dominated by spatial and spectral diffusion, where the spatial diffusion is controlled by elastic resonant scattering from the $\text{Cr}^{3+} {}^2E$ excited electronic states of the single ions, and the spectral diffusion (frequency shifting) is due to Raman scattering by exchange coupled Cr^{3+} pair states.

An exchange-coupled pair-state model was developed

which goes beyond previous models for ruby. In the earlier Meltzer-Rives¹ model, only site-site energy transfer was considered and it was necessary to assume an exchange parameter J which was smaller than estimates from other work. That model was successful only at large N^* . The de Wijn-Dijkhuis model⁶ considered only the inelastic Raman scattering of a phonon, and ignored the site-site transfer entirely. It was successful at fitting the intermediate range of N^* . Both models chose arbitrary values for the pair-state energy levels and neither considered the role of the ground-state splitting properly.

In the pair-state model, developed here, wave functions for the exchange-coupled pair were constructed which properly take into account the $\text{Cr}^{3+} C_{3v}$ point-group symmetry. Eigenvalues and eigenfunctions were calculated for a range of typical pairs where the exchange and site-site energy mismatch were treated on an equal footing. Site-site transfer, although it occurs only infrequently, was included and the effect of the ground state multiplet was explicitly considered. The relative transition probabilities among these eigenfunctions were determined in order to obtain the probabilities for frequency shifting Raman scattering processes among the pair states. The phonon loss rates were determined by computer simulations which included both the spatial and spectral dynamics of the phonons. In addition, the model was extended to alexandrite.

The major approximations in the model are the neglect of mixing of the 4T_2 and 2E states,²⁵ the estimation of the exchange parameters J_{ij} the omission of biquadratic exchange and the representation of the problem using the most probable off-diagonal exchange matrix elements. Without additional information about the J_{ij} or the biquadratic exchange parameters J_{ijj} we cannot substantially improve the model.

This model produced an excellent fit to the experimental data for ruby, as well as for alexandrite, for values of the exchange parameter consistent with earlier estimates.^{12,13} In addition the pair-state model predicts the fact that the spectral shifting in ruby is dominated by the ${}^4A_2(\pm\frac{1}{2})$ pair states, relative to the ${}^4A_2(\pm\frac{3}{2})$ states, and this was subsequently verified in experiments which measured the phonon lifetime as a function of temperature in a magnetic field. Although the pair-state model was not derived from first principles, it provides an improved insight into the spectral diffusion process in both ruby and alexandrite.

ACKNOWLEDGMENTS

We wish to thank Allied Corporation for providing the alexandrite samples and the National Science Foundation under Grant No. DMR-8514001 for partial support of this work.

*Present address: Department of Chemistry, Cornell University, Ithaca, NY 14853.

¹R. S. Meltzer, J. E. Rives, and W. C. Egbert, *Phys. Rev. B* **25**, 3026 (1982).

²G. F. Pauli, K. F. Renk, G. Klimke, and H. J. Kreuzer, *Phys.*

Status Solidi B **95**, 503 (1979).

³A. A. Kaplyanskii and S. A. Basun, in *Nonequilibrium Phonons in Nonmetallic Crystals*, edited by W. Eisenmenger and A. A. Kaplyanskii (Elsevier, New York, 1986), pp. 373–453.

⁴A. A. Kaplyanskii, S. A. Basun, and V. L. Shekhtman, in

- Light Scattering in Solids*, edited by J. L. Birman, H. Z. Cummins, and K. K. Rebane (Plenum, New York, 1979), pp. 95–111.
- ⁵J. I. Dijkhuis and H. W. de Wijn, *Solid State Commun.* **31**, 39 (1979).
- ⁶R. J. G. Goossens, J. I. Dijkhuis, and H. W. de Wijn, *Phys. Rev. B* **32**, 7065 (1985).
- ⁷R. J. G. Goossens, J. I. Dijkhuis, and H. W. de Wijn, *Phys. Rev.* **32**, 5163 (1985).
- ⁸K. F. Renk and J. Deisenhofer, *Phys. Rev. Lett.* **26**, 764 (1971).
- ⁹S. Majetich, J. E. Rives and R. S. Meltzer, in *Phonon Scattering in Condensed Matter V*, edited by A. C. Anderson and J. P. Wolfe (Springer-Verlag, Heidelberg, 1985), pp. 338–340.
- ¹⁰U. Happek, T. Holstein, and K. F. Renk, *Phys. Rev. Lett.* **54**, 2091 (1985).
- ¹¹U. Happek, T. Holstein, and K. F. Renk, *Phys. Rev. B* **34**, 8898 (1986).
- ¹²J. W. Allen, R. M. Macfarlane, and R. L. White, *Phys. Rev.* **179**, 523 (1966).
- ¹³R. J. Birgeneau, *J. Chem. Phys.* **50**, 4282 (1971).
- ¹⁴S. A. Basun, A. A. Kaplyanskii, and S. P. Feofilov, *Fiz. Tverd. Tela (Leningrad)* **28**, 3616 (1986) [*Sov. Phys.—Solid State* **28**, 2038 (1986)].
- ¹⁵M. J. van Dort, J. I. Dijkhuis, and H. W. de Wijn, *J. Lumin.* **38**, 217 (1987).
- ¹⁶J. R. Wietfeldt, D. S. Moore, B. M. Tissue, and J. C. Wright, *Phys. Rev. B* **33**, 5788 (1986).
- ¹⁷J. E. Rives and R. S. Meltzer, *Phys. Rev. B* **16**, 1808 (1977).
- ¹⁸A value of $T_1 = 0.4$ ns in alexandrite was obtained from measurements of the temperature dependence of the homogeneous linewidth. See D. Boye, S. Majetich, J. E. Rives, R. S. Meltzer, and R. M. Macfarlane, in *International Quantum Electronics Conference*, Baltimore, 1987 (unpublished).
- ¹⁹J. C. Walling, O. G. Peterson, H. P. Jossen, R. C. Morris, and E. W. O'Dell, *IEEE J. Quantum Electron.* **QE-16**, 1302 (1980).
- ²⁰D. Sox, S. Majetich, J. E. Rives, and R. S. Meltzer, *J. Phys. Colloq. C7*, **46**, 493 (1985).
- ²¹M. Lax, V. Narayanamurti, R. C. Fulton, and N. Holzwarth, in *Phonon Scattering in Condensed Matter V*, edited by A. C. Anderson and J. P. Wolfe (Springer-Verlag, Heidelberg, 1986), pp. 335–337.
- ²²R. D. Present, *The Kinetic Theory of Gases* (McGraw-Hill, New York, 1958), pp. 28 and 29.
- ²³Kaplyanskii *et al.* (Ref. 3) have noted a near resonance between levels of the fourth-nearest neighbors in ruby and the 2E levels (28.8 cm^{-1} versus 29.2 cm^{-1}). The pair-state model shows that most of the pair states which are active in spectral diffusion are separated from the single-ion frequency by less than 0.4 cm^{-1} . Due to the extremely narrow resonance width in ruby (0.02 cm^{-1}), the fourth-nearest neighbors will, therefore, be out of resonance with the vast majority of single ions.
- ²⁴Nai Li Huang, *Phys. Rev. B* **1**, 945 (1970).
- ²⁵S. Sugano, Y. Tanabe, and H. Kamimura, *Multiplets of Transition-Metal Ions in Crystals* (Academic, New York, 1970).
- ²⁶S. K. Lyo, *Phys. Rev. B* **3**, 3331 (1971).
- ²⁷R. C. Powell, L. Xi, X. Gang, G. J. Quarles, and J. C. Walling, *Phys. Rev. B* **32**, 2788 (1985).
- ²⁸M. Blume, R. Orbach, A. Kiel, and S. Geschwind, *Phys. Rev. A* **139**, 314 (1965).
- ²⁹J. I. Dijkhuis and H. W. de Wijn, *Phys. Rev. B* **20**, 3615 (1979).